Nano- and Micro-Scale Temperature Measurements Using Laser-Induced Fluorescence Thermometry

by

Christine Tomforde

A Thesis Presented in Partial Fulfillment
of the Requirements for the Degree
Master of Science

Approved July 2011 by the
Graduate Supervisory Committee:

Patrick Phelan, Chair
Lenore Dai
Ronald Adrian

ARIZONA STATE UNIVERSITY

August 2011

ABSTRACT

A method of determining nanoparticle temperature through fluorescence intensity levels is described. Intracellular processes are often tracked through the use of fluorescence tagging, and ideal temperatures for many of these processes are unknown. Through the use of fluorescence-based thermometry, cellular processes such as intracellular enzyme movement can be studied and their respective temperatures established simultaneously. Polystyrene and silica nanoparticles are synthesized with a variety of temperature-sensitive dyes such as BODIPY, rose Bengal, Rhodamine dyes 6G, 700, and 800, and Nile Blue A and Nile Red. Photographs are taken with a QImaging QM1 Questar EXi Retiga camera while particles are heated from 25 to 70 C and excited at 532 nm with a Coherent DPSS-532 laser. Photographs are converted to intensity images in MATLAB and analyzed for fluorescence intensity, and plots are generated in MATLAB to describe each dye's intensity vs temperature. Regression curves are created to describe change in fluorescence intensity over temperature. Dyes are compared as nanoparticle core material is varied. Large particles are also created to match the camera's optical resolution capabilities, and it is established that intensity values increase proportionally with nanoparticle size. Nile Red yielded the closest-fit model, with R^2 values greater than 0.99 for a second-order polynomial fit. By contrast, Rhodamine 6G only yielded an R2 value of 0.88 for a third-order polynomial fit, making it the least reliable dye for temperature measurements using the polynomial model. Of particular interest in this work is Nile Blue A, whose fluorescence-temperature curve yielded a much different

shape from the other dyes. It is recommended that future work describe a broader range of dyes and nanoparticle sizes, and use multiple excitation wavelengths to better quantify each dye's quantum efficiency. Further research into the effects of nanoparticle size on fluorescence intensity levels should be considered as the particles used here greatly exceed 2 µm. In addition, Nile Blue A should be further investigated as to why its fluorescence-temperature curve did not take on a characteristic shape for a temperature-sensitive dye in these experiments.

ACKNOWLEDGMENTS

I would like to thank my advisor, Dr. Patrick Phelan, for his support and insight throughout this project. I would also like to thank Dr. Ronald Adrian for the use of his lab and equipment, and Dr. Lenore Dai for the use of her lab and assistance with literature review. I would also like to thank Sriya Sanyal for her tireless assistance with lab supplies and insight into future research, and Andrey Gunawan for his assistance with experiment setup. I would also like to thank Dr. Bruce Steele for assistance in procuring lab equipment.

TABLE OF CONTENTS

CHAPTER Page

LIST OF TABLES

LIST OF FIGURES

Figure Page

CHAPTER 1

INTRODUCTION AND LITERATURE REVIEW

1.1 Use of fluorescence tagging in intracellular process tracking

A variety of nanoparticle materials and dyes are used in combination to establish and describe a correlation between nanoparticle temperature and dye fluorescence intensity. This approach allows for temperature determination without the use of a thermocouple or thermometer and can be used in nano- or micro-scale systems such as cellular processes. The reliability, resolution, and range of each combination of particle material and dye is discussed.

Fluorescence tagging has long been used to track molecules of interest in biological systems, particularly in cellular processes [1-3]. A fluorescent chromophore such as a dye is bonded to the molecule of interest, often an enzyme or other protein, and a scanning electron microscope or other imaging technology is used to record the position of the tag at various points in time to trace its movements within or between cells. With the use of a temperature-sensitive dye, such tags could become temperature indicators as well as spatial indicators [4]. This method is of especial interest for tracking intracellular temperatures, as medical procedures such as thermal therapy rely on accurate temperature indicators to monitor triggered cellular necrosis in cancerous cells [5]. In addition, fluorescence tags are often used in polymerase chain reactions to determine optimal temperature to amplify DNA, an invaluable precursor to genetic testing and cloning [6-11].

1.2. Fluorescence phenomena and mechanisms

Following the work of Ross et al. [4], a temperature determination method is developed using fluorescent laser dyes and a charge-coupled device (CCD) camera. However, Ross et al focus on micro- rather than nano-fluidic systems, and obtain a temperature resolution of 3 or 3.5 C. The data presented here have a temperature resolution of ±1 C, as a scientific thermometer is used to verify temperatures across all fluorescence data and images while Ross et al. only have established reference data at 25 C. Therefore, some systematic uncertainty is introduced, and is of particular concern for images obtained far from the reference temperature.

Lan et al [12] have developed a method for ex-situ temperature determination, which eliminates the need for real-time data analysis. In the work presented here real-time data acquisition is preferred, as ex-situ methods can only establish temperature at a given point in time, usually the maximum temperature obtained during the course of the experiment. While this method may be favorable for single-process thermometry tracking, it would be limiting in the case of an intracellular molecule that is expected to undergo multiple processes at multiple temperatures [12].

Some attempts at creating three-dimensional temperature profiles have been made [13,14]. One of particular interest to intracellular tracking follows Park and Choi's method, which takes into account the Brownian motion of the particles by relating the particle movement through a given field to the particle's fluorescence levels at certain points in the field [14].

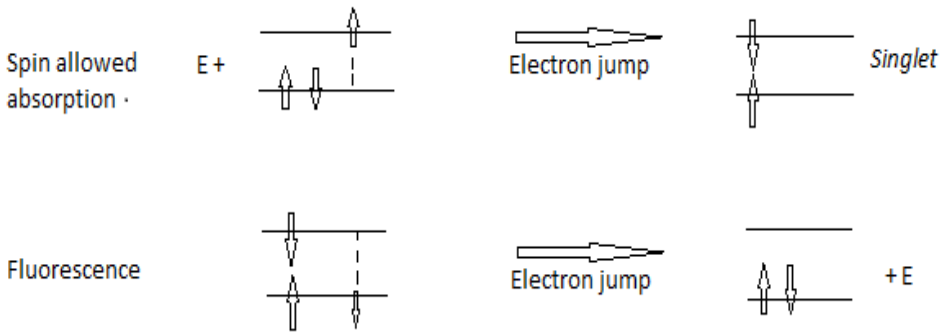

Figure 1. Schematic of fluorescence mechanism, taken from [13].

When energy strikes an atom, electrons are excited and elevate to a higher energy state. By Planck's law, this energy equates to

$$E = h\nu = hc/\lambda \quad (1)$$

Here E represents the total energy input, c is the speed of light, and λ the wavelength of the incident light. Due to the inverse relationship between wavelength and energy, higher excitation wavelengths indicate lower energy requirements for excitation. The dyes used in this work have published excitation wavelengths that are used as a benchmark minimum for energy requirements. Because the laser used is single-wavelength and emits at 532 nm, dyes used in this case must have excitation requirements at or above 532 nm. Electrons losing this energy return to their ground state, emitting roughly the energy used to excite them. This energy emission is now lower than the original energy input due to the energy loss associated with the electron's return to ground state. Thus, λ is now a longer wavelength than that used for excitation. This is illustrated in Figure 1. Due to the camera's sensitivities to the laser, a cutoff filter is used to cancel wavelengths shorter than 560 nm.

This can be used to determine the amount of fluorescence detected by the camera when photographing dyes. Consequently, only dyes with excitation wavelengths longer than or equivalent to the laser wavelength can be used; in addition, dyes' emission spectra must have substantial levels above 560 nm to be detected.

CHAPTER 2

OUTLINE AND RESEARCH OBJECTIVES

Methods for synthesizing two different varieties of nanoparticles are presented, with six different dyes to be investigated. A seventh dye is included for comparison, as literature is already available for BODIPY fluorescence-vs-temperature curves [13]. Data collection and processing techniques are discussed, and curves for fluorescence vs temperature for six dyes are produced. Due to limitations in the optics equipment available, nanoparticles are later created with much longer aggregation times, yielding micro-scale materials on the order of 2 mm. Results for these microparticles are compared with known nanoparticle data to establish proportionality between the sizes of particles given here and the actual sizes to be used in later applications. Curve-fitting is performed to describe fluorescence as a function of temperature so future work may determine nanoparticle temperature based on fluorescence images of any of these dyes rather than thermocouples or thermometers. In the case of intracellular tracking, images may be able to simultaneously yield both location and temperature data for a variety of biological molecules.

CHAPTER 3

EXPERIMENTAL PROCEDURE

3.1.1. Polystyrene nanoparticle synthesis. Polystyrene nanoparticles are created using the materials outlined in Table 1.

Table 1. Materials list for polystyrene nanoparticle synthesis.

30 g HPLC water
12.2 g IPA-ST colloidal silica in isopropanol
4.432 g Styrene monomer
.0036 g VA-086 initiator
VWR condenser
ThermoScientific hot plate
VWR scientific thermometer 61066-126
Nitrogen source
Airtight rubber sleeves
3-way valve flask
Sterile pipettes
Sterile stirrers
.001 g dye

The dyes used in particle synthesis here are listed in Table 2. Dyes were chosen based on prior usage in similar applications [1-3].

Table 2. Dyes used in particle synthesis

Rhodamine 6G
Rhodamine 700
Rhodamine 800
Rose Bengal
BODIPY
Nile Red
Nile Blue A

BODIPY, or boron-dipyrromethene, is often used for fluorescence tagging of proteins, oligonucleotides, and dextrans [16], and as such is a good candidate

for fluorescence thermometry applications. However, its peak excitation occurs below 532 nm and only small levels of fluorescence are detectable with the filter used in this work.

Rose Bengal is already used in cancer diagnosis and treatments, and Chan and Chan are currently developing a method of creating nano-sutures using the dye [17].

Nile Red is a common, inexpensive dye used for staining intracellular lipids; however, its emission spectra are highly solvent-dependent. Here water is used as the main solvent as this is the medium in which biological processes occur. However, future work should consider whether common laboratory cleaning agents such as ethanol or isopropanol are present, as small amounts of these solvents can easily contaminate results [18].

Nile Blue A, a precursor of Nile Red, is also used for staining intracellular lipids and fatty acids [19]. It is similarly common and inexpensive, and also used here for comparison between the two Nile dyes.

All of the Rhodamine dyes used here are commonly found in immunoassays such as ELISA processes, or enzyme-linked immunosorbent assays, as they are used in tagging antibodies and antigens [20]. As they have similar chemical structures but different peak excitation wavelengths, they are chosen here with the expectation of obtaining similar fluorescence-temperature curves. The dyes with lower excitation wavelengths are expected to have higher fluorescence intensity levels while maintaining a proportional shape to the less excitable fluorophores.

All of the dyes used here are selected for excitation wavelengths longer than 532 nm so the laser can provide adequate excitation energy, and all dyes exhibit a high amount of emission at wavelengths longer than 560 nm so that they can be detected through the filter in the camera. A plot of the camera's transmission levels near the cutoff wavelength is shown in Figure 2.

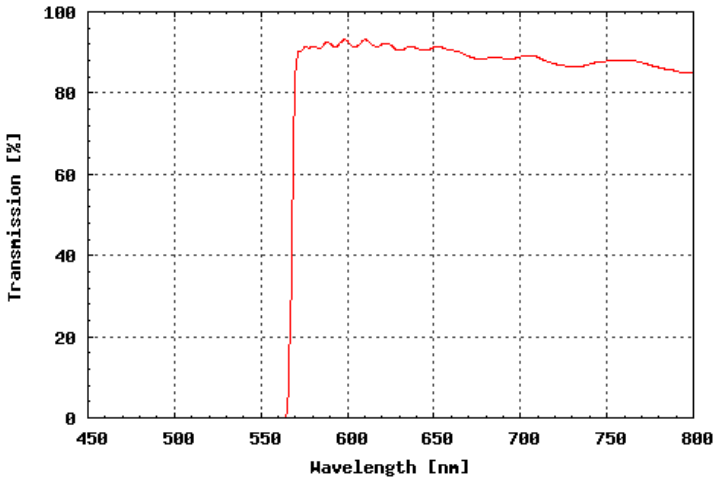

Figure 2. Plot of cutoff filter's transmission at varying wavelengths. Taken from [15]. Dyes used in this work must have substantial levels of fluorescence emission above 560 nm to avoid being canceled by filter.

Styrene, HPLC, silica, and dye are weighed in situ as shown in Figure 3 and mixed with mechanical stirrer for two minutes. The contents are then poured into a three-way valve flask with a stir bar, which is then fitted with a condenser in one valve, and rubber sleeves on the remaining valves. Due to nitrogen's inability to react with nanoparticle materials, a nitrogen source is connected to the flask and inserted through a rubber sleeve in order to achieve an airtight system.

A thermometer is inserted through the other sleeve to monitor temperature, as seen in Figure 4. The hot plate is allowed to heat the flask until the contents reach 70 C, at which point the initiator can be added. Due to its high reactivity and resulting safety concerns, the initiator must be added to HPLC inside a separate vial and mixed, then added via pipette to the flask. The sleeves are replaced and then heat is reduced to maintain a constant temperature of 70 C for aggregation time. Figure 5 shows a schematic of this process.

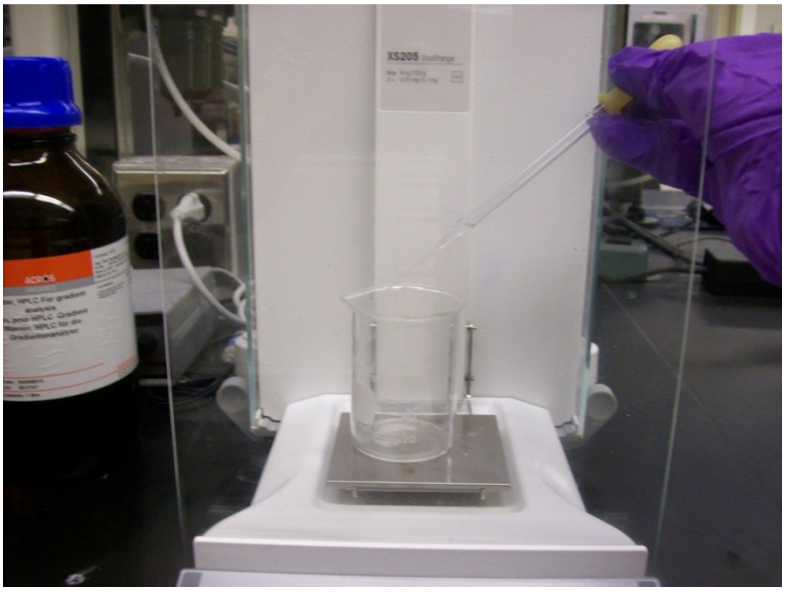

Figure 3. Materials are weighed in situ prior to mixing

Figure 4. Nanoparticle polymerization. The valve on the left connects to a nitrogen tank, while the temperature is monitored using the thermometer on the right. The condenser ensures the solvent does not boil off.

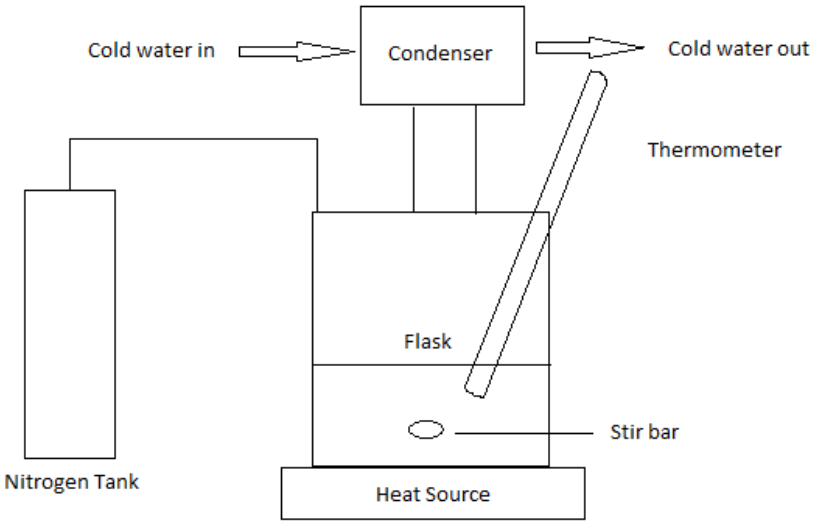

Figure 5. Schematic of setup depicted in Figure 4.

This process of particle formation relies on a polymerization reaction described by Schellenberg [20]. The process begins with a styrene monomer that connects in chains of many thousand to form strings or sheets, depending on the positioning of the chiral arms [21].

The polymerization occurs when a single carbon bond in the vinyl group of the styrene monomer breaks and is replaced by the stronger double bond. Initiation of this process is achieved here with VA-086, or 2,2'-Azobis[2-methyl-N-(2-hydroxyethyl) propionamide]. The initiator is shown in Figure 6, and the styrene monomer in Figure 7. The polymerization process is shown in Figure 8.

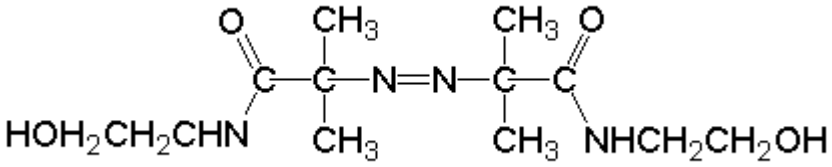

Figure 6. Initiator used to catalyze polymerization process. Taken from [22].

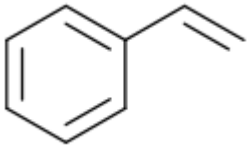

Figure 7. Styrene monomer prior to polymerization. The vinyl group on the end is broken and more monomers are added. Taken from [23].

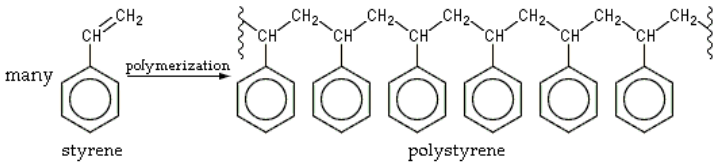

Figure 8. Polystyrene formation process. Taken from [24].

Aggregation times are varied to achieve a range of particle sizes; in the case of this experiment they are varied from five to seven hours. After polymerization is completed, the mix is poured into centrifuge tubes and centrifuged at 8000 RPM for 8 minutes; then the supernatant is poured off and the volume replaced with deionized water. If no pellet is visible, or the supernatant is particularly cloudy a second centrifugation under the same settings is performed. An example of a visible pellet is shown in Figure 9.

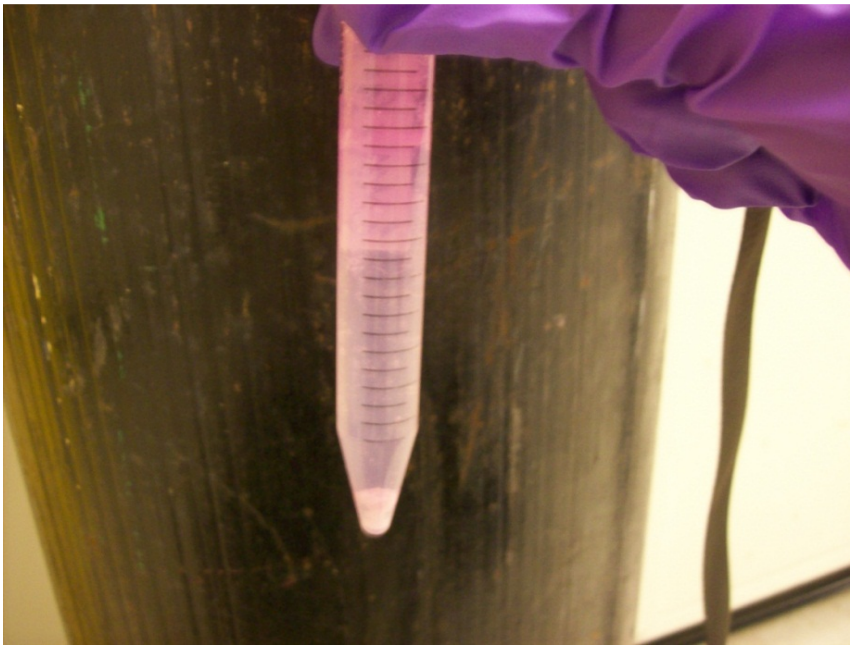

Figure 9. Visible polystyrene pellets observed after centrifugation

3.1.2. Dimethyl methyl acrylamide particle synthesis. The procedure for creating dMMA nanoparticles is identical to that of creating polystyrene particles, with the substitution of 2.216 g of dMMA dimers for half of the amount of styrene used in polystyrene synthesis. In other words, rather than using 4.432 g of styrene, 2.216 g of styrene and 2.216 g of dMMA are used.

3.2. Fluorescence Inducement and Detection Methods

Materials used in data collection are given in Table 3. For detecting fluorescence levels, the centrifuged solution is poured into polystyrene or poly (methyl methylacrylamide) cuvettes which are placed on a hot plate. A thermometer is clamped over the cuvette so the bulb is immersed in the fluid to confirm the hot plate temperature during the experiment. The laser is aligned so the beam is normal to the cuvette surface, and the camera is similarly aligned to the same region of the cuvette. As the cuvette is heated, pictures are taken at each change in degree Celsius to obtain photos across the temperature range. A "baseline" photograph, without the laser effect, is also taken to cancel the laser's signal during subsequent photograph analysis. This allows for assurance that the detected signal in the photographs occurs from the fluorescence phenomenon rather than a general heating of the dye. The experimental setup is shown in Figures 10 and 11.

Table 3. Materials for data collection

Coherent DPSS-532 laser
Q Imaging Questar QM1 Retiga EXi camera
Polystyrene cuvettes
PMMA cuvettes
VWR Scientific thermometer 61066-126
ThermoScientific hot plate

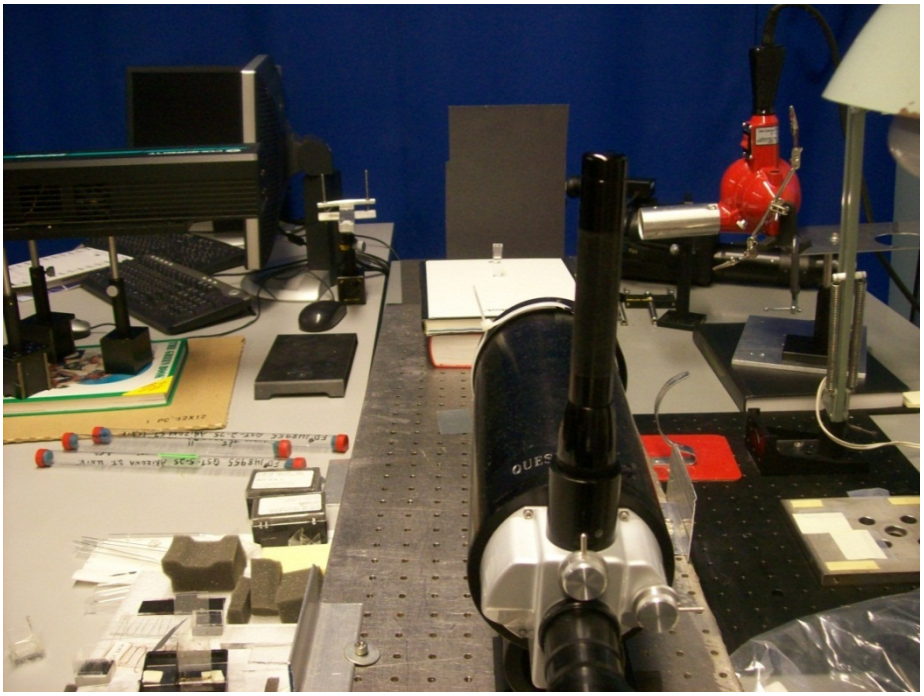

Figure 10. Experimental setup for data collection. Cuvette is in the background of photograph, while camera is in the foreground. Laser is located to the left of the cuvette

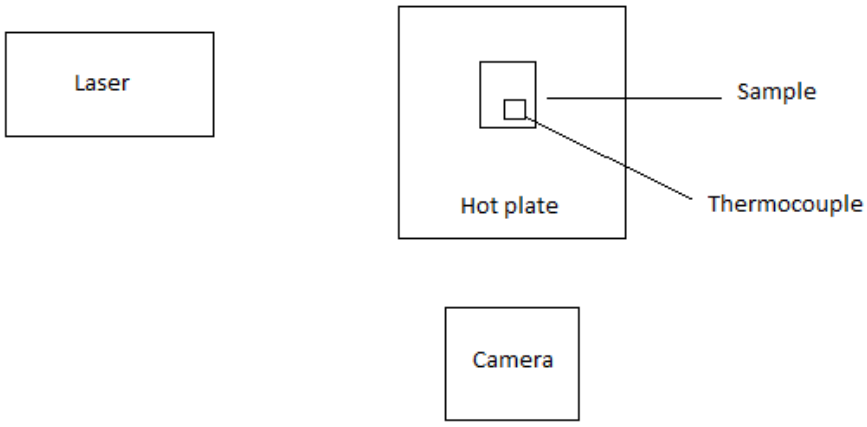

Figure 11. Schematic of experimental setup for data collection

CHAPTER 4

DATA PROCESSING METHODS

4.1 Image Processing

Image processing is accomplished with a MATLAB script. Similar to the use of a LabView imaging program in [4] images are read to files and mapped into an intensity matrix, which assigns an intensity value to each pixel of the image. This allows the operator to determine specific sections of the image he would like to examine and define them with the matrix indices assigned by MATLAB. MATLAB then assigns an "intensity" rating to each pixel, allowing MATLAB to recreate the image by displaying the intensity of each pixel in the ordered matrix. This also allows the operator to create normalized intensity images, where the lowest-intensity pixel in the image is assigned a value (usually 0) and the highest-intensity pixel another (usually 1). Images can be stored to MATLAB in a number of ways, depending on whether the operator wants a truecolor image or grayscale. In the case of a class double matrix for a truecolor image, each element in the matrix (a vector with three coordinates) corresponds to each pixel of the image, with the three coordinates representing red, green, and blue intensities, respectively. This allows MATLAB to read the image as an intensity matrix but save it as a colormap.

Once the image is converted to a matrix, MATLAB can subtract matrices or images from each other. This is especially helpful in the case of a laser-induced fluorescence, where it is necessary to distinguish the fluorescence of the particles from the laser's signal. In this case a picture can be taken without

the particles (a no-fluorescence baseline) and without the laser (a no-laser signal baseline) and these images can be subtracted accordingly from the experimental camera photographs of the particles fluorescing under the laser. In this way the operator can track only the fluorescence phenomena in the images without added laser signals. This is also helpful for removing spots or lint that may be present on the camera, as any noise present in all pictures will be subtracted from itself during image processing.

Another benefit of using MATLAB to track changes in image intensity is that the maximum intensity can be identified, and the location of the pixels returned. This is useful in tracking which sections of the image fluoresce the brightest at various points throughout the experiment. In particular, if a particle is in motion through the cross-section of interest, it can be identified and tracked as long as it is inside the field of vision of the camera. This may be of especial interest for tracking the fluorescent tags applied to intracellular molecules if the fate or location of the molecule is being studied. A flowchart of data processing procedures is shown in Figure 12.

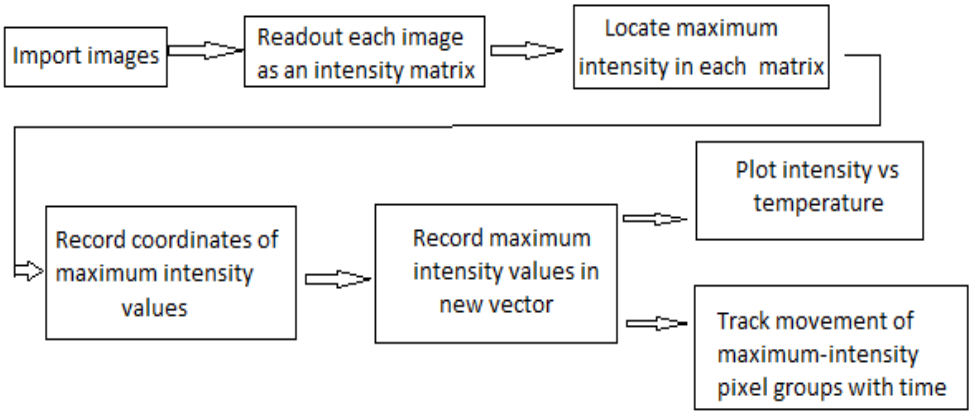

Figure 12. Flowchart of data processing procedures

4.2 Regression Curve Generation and Statistical Analysis

Once intensity plots are generated, data are imported to Microsoft Excel and curve-fitting tools are used. As most plots reached a peak intensity between 40 and 50 C, curve fits are split between the temperature range prior to the peak and the range after the peak. Excel's R^2 meter is used to measure the effectiveness of the fit. Equations and R^2 values are reported in Table 4.

CHAPTER 5

RESULTS AND DISCUSSION

5.1. Intensity-temperature curves for polystyrene particles

The polystyrene and BODIPY plot followed the shape expected from [25]. Figure 13 shows the dye reaching their peak intensity around 43 C, then decreasing and following a roughly linear shape afterward. Ordinate axis units are arbitrary units assigned by MATLAB. Both literature [25] and experimental results are included for comparison.

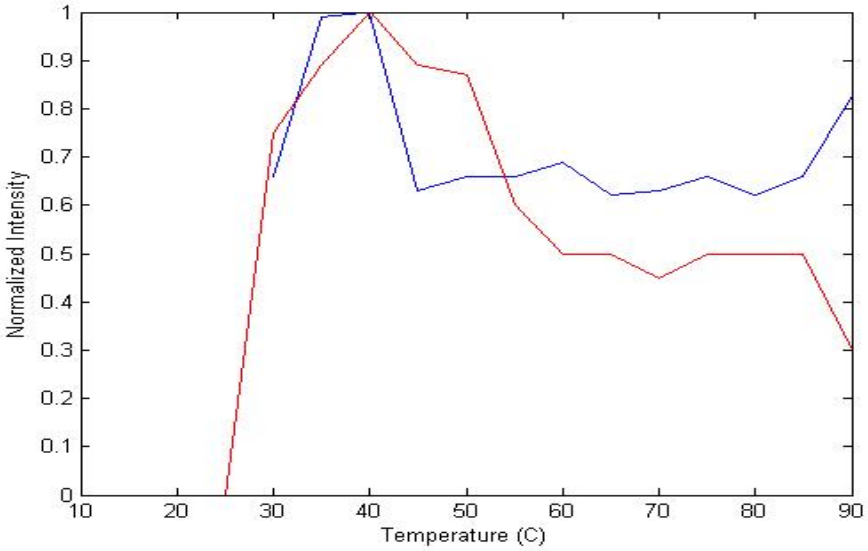

Figure 13. Intensity plot of polystyrene particles with BODIPY dye.

Rose Bengal followed a roughly similar shape as seen in Figure 14; however, the peak intensity occurred around 55 C. Rose Bengal also differed in having a much larger disparity between peak intensity and final intensity.

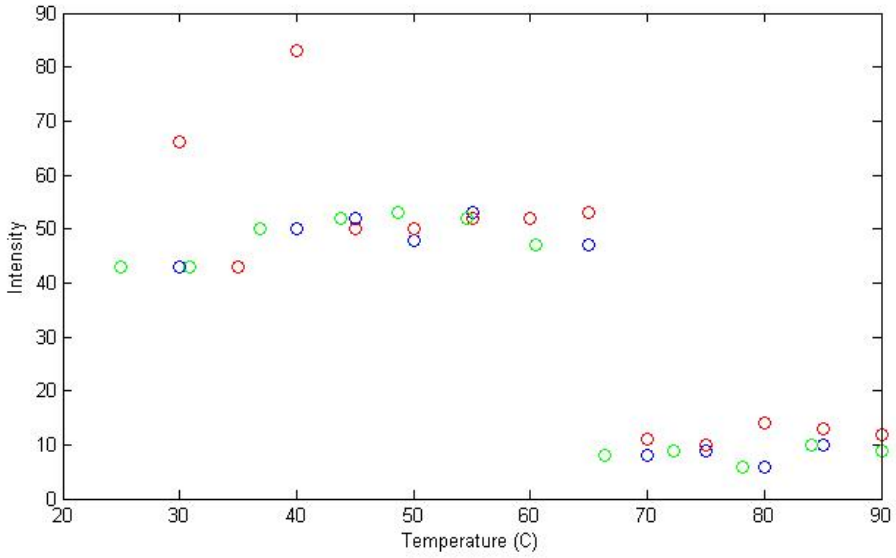

Figure 14. Polystyrene with Rose Bengal

The rhodamine dyes showed a markedly different approach to peak intensity. Rather than following a flat or concave-down parabola prior to reaching peak intensity, Rhodamine 700 appeared as a concave-up parabola prior to reaching peak as seen in Figure 15. After reaching peak intensity, Rhodamine 700 decreased rapidly and then leveled off, similar to the above graphs. Maximum intensity occurred at 43 C similar to BODIPY.

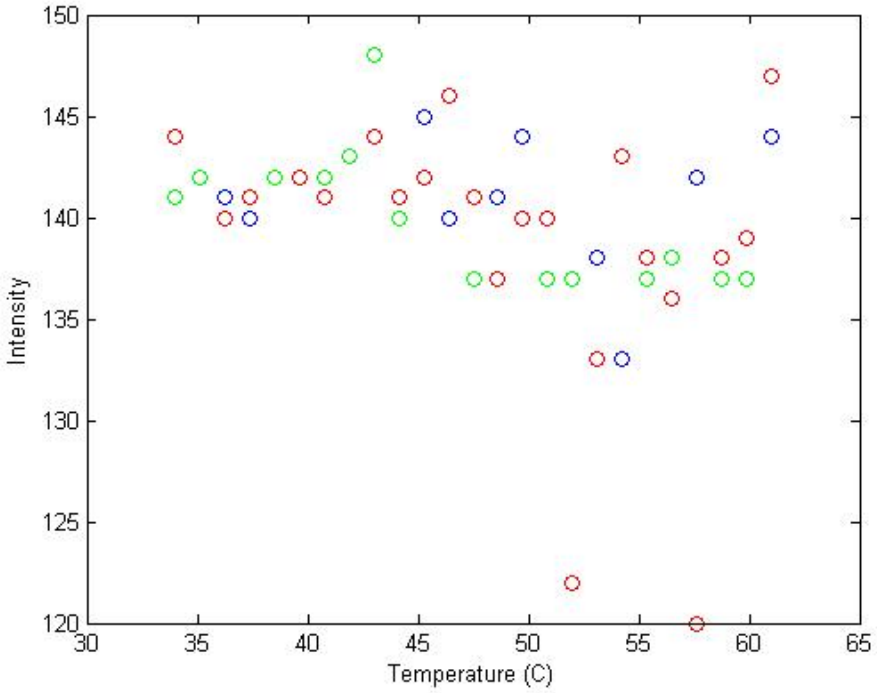

Figure 15. Polystyrene with Rhodamine 700

Rhodamine 800 displayed a similar concave-down shape as it reached maximum intensity in Figure 16; however, afterwards intensity levels dropped to near zero and stayed negligible to the end of the temperature range.

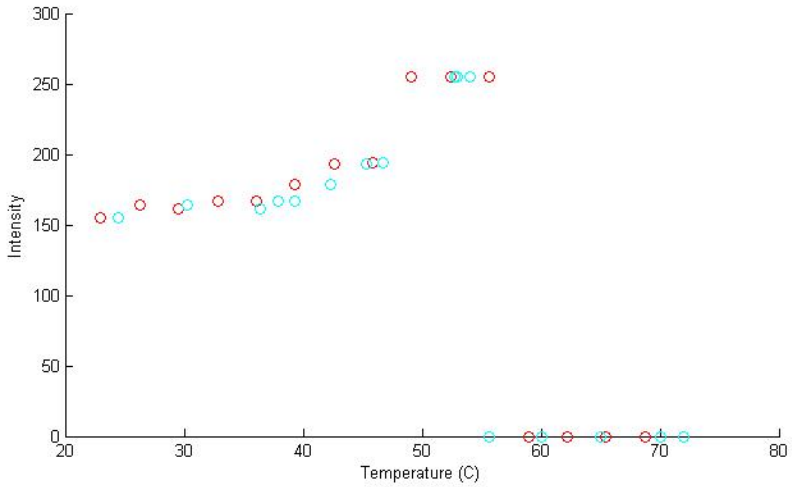

Figure 16. Polystyrene with Rhodamine 800

Rhodamine 6G displayed the most issues with curve-fitting. The shape remained similar to the other rhodamine dyes approaching the maximum intensity, which occurred at 53 C, but only decreased to intensity levels higher than those reached before maximum intensity. This is seen in Figure 17.

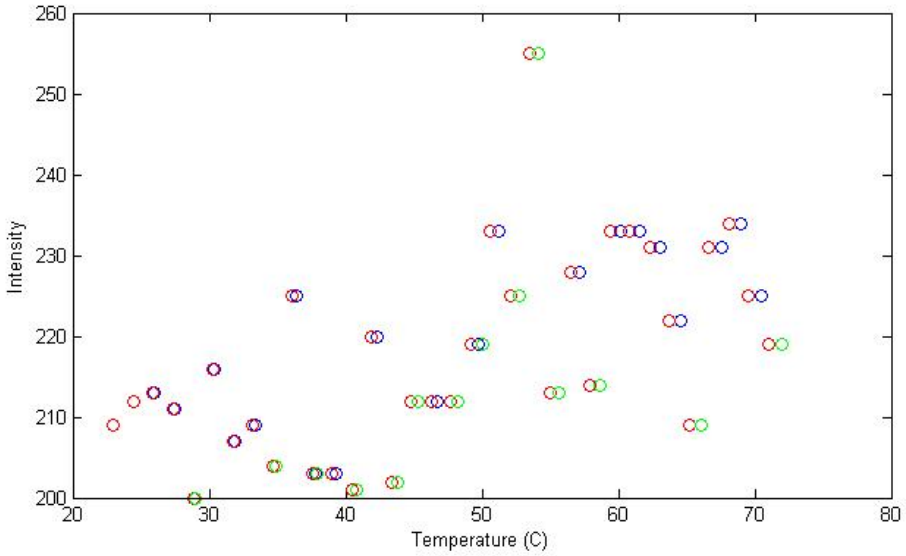

Figure 17. Polystyrene with Rhodamine 6G

Nile red displayed the most gradual decrease from maximum intensity at 46 C, eventually reaching zero; however, it began to increase again after 67 C as seen in Figure 18.

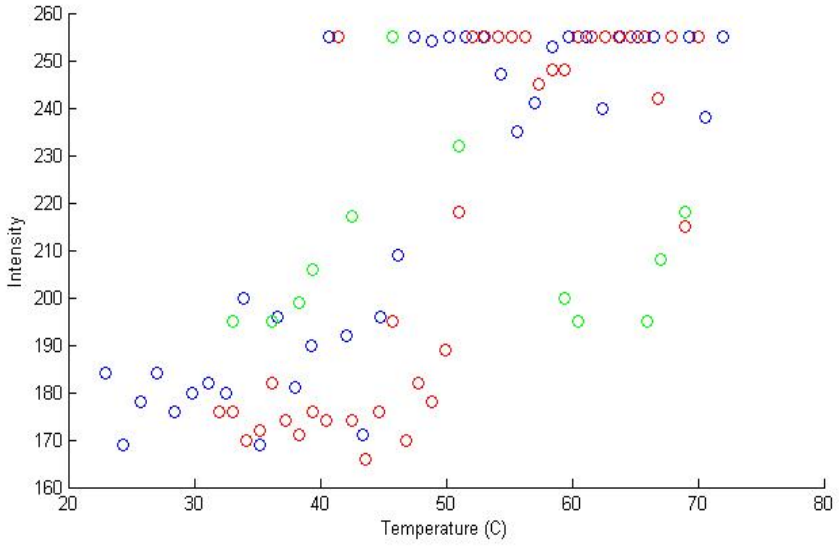

Figure 18. Polystyrene with Nile Red

Nile Blue A was the only dye that did not reach a peak intensity or follow the expected shape. Instead, in all experiments it kept increasing past the temperature range of the experiments. Figure 19 shows the dye increasing indefinitely. Data were noisy and unstable for all experiments; however, a definite increasing trend can be seen.

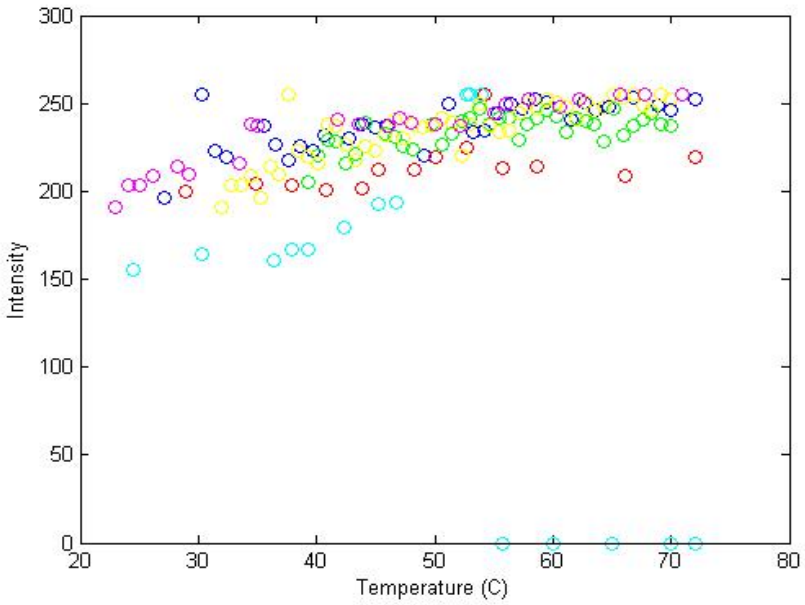

Figure 19. Polystyrene with Nile Blue

Curve-fitting was then performed in Excel and MATLAB for all dyes. For greater accuracy regression curves were calculated separately for temperatures prior to maximum and after maximum. Plots are presented here with data points used to make curves represented by open circles. Table 4 shows equations used for fitting the data prior to reaching maximum intensity and R^2 values for each temperature range. Figures 20-26 show the original intensity data points with overlaid regression curves.

Table 4. Curve fits for dyes prior to reaching maximum

Dye	Equation 1	R^2	Temperature range
BODIPY	$y = -1.1171x^2 + 89.751x - 1643$	0.9449	30 C - 60 C
Rose Bengal	$y = -0.024x^2 + 2.2416x + 0.1491$	0.8685	25 C - 60 C
Rhodamine 700	$y = 0.0619x^3 - 6.9968x^2 + 262.84x - 3142$	0.9757	34 C - 43 C
Rhodamine 800	$y = 0.1842x^2 - 11.272x + 327.64$	0.9755	25 C - 55 C
Rhodamine 6G	$y = 0.011x^3 - 1.2486x^2 + 46.699x - 373.82$	0.8817	29 C - 54 C
Nile Red	$y = 0.4738x^2 - 32.937x + 571.69$	0.9937	33 C - 46 C
Nile Blue A	$y = 0.0013x^3 - 0.2047x^2 + 11.371x + 26.58$	0.936	23 C - 71 C

As seen in Table 4, Rose Bengal and Rhodamine 6G both were poor fits for the data, with R^2 values lower than 0.9 even when Rhodamine 6G was fitted with a third-order polynomial. The closest fit occurred for Nile Red, with an R^2 value of 0.9937.

Due to Rhodamine 800 declining to negligible values after maximum, and the increasing shape of Nile Blue A, curve fits were not performed for this section of the data for these dyes. Table 5 shows the fits for the post-maximum sections of temperature data for the remaining dyes.

Table 5. Curve fits for dyes after reaching maximum

Dye	Equation 2	R^2	Temperature range
BODIPY	$y = -0.64x + 94.8$	0.8127	60 C -70 C
Rose Bengal	$y = -0.0574x^2 + 8.1284x - 278.6$	0.99999	60 C - 70 C
Rhodamine700	$y = -0.0066x^3 + 1.0526x^2 - 55.611x + 1113$	0.9278	43 C - 70 C
Rhodamine 6G	$y = -0.0427x^3 + 8.4357x^2 - 553.26x + 12244$	0.83	54 C - 70 C
Nile Red	$y = 0.1709x^2 - 22.305x + 726.18$	0.9897	46 C - 70 C

Rhodamine 6G again displays a poor fit, with an R^2 value of only 0.83. However, the BODIPY dye is the worst fit for this section of the data with a value

of 0.81. This is likely due to higher amounts of noise in the data after temperatures reached 43 C than prior to reaching this temperature.

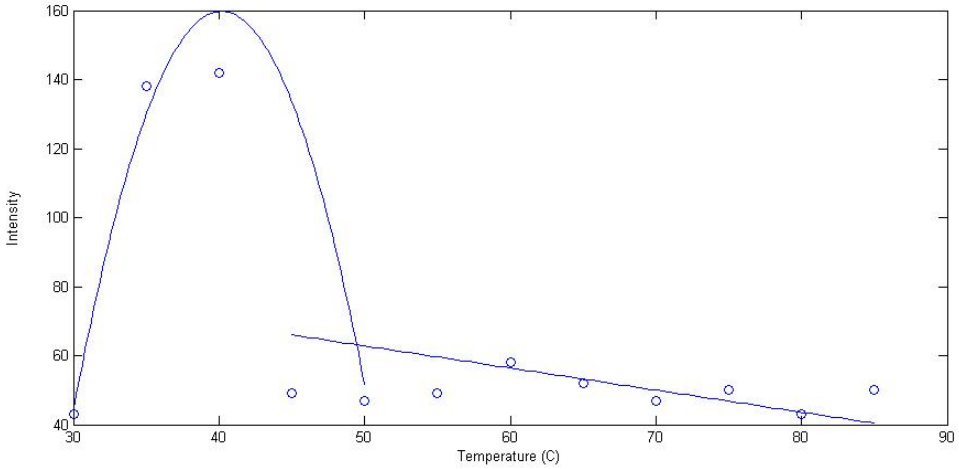

Figure 20. Polystyrene with BODIPY dye, modeled by parabola and line

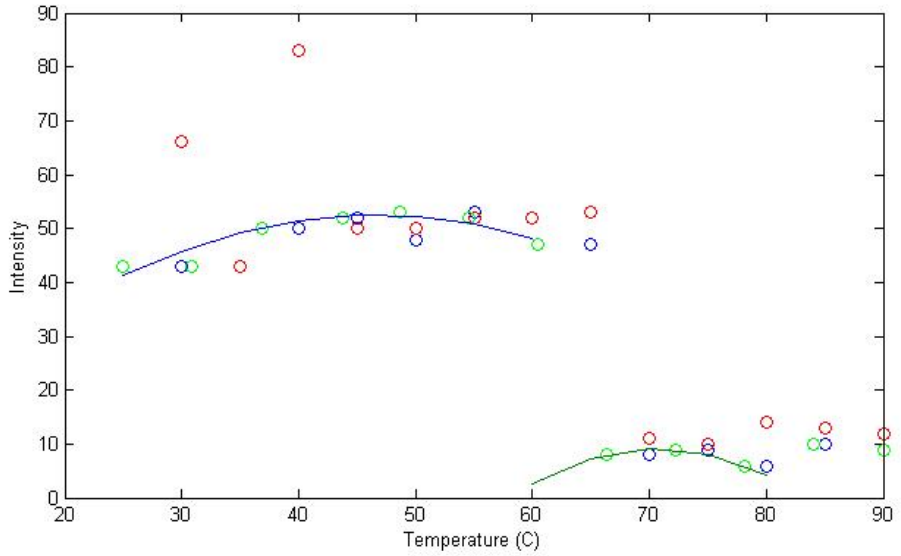

Figure 21. Polystyrene with Rose Bengal dye, modeled by two parabolas

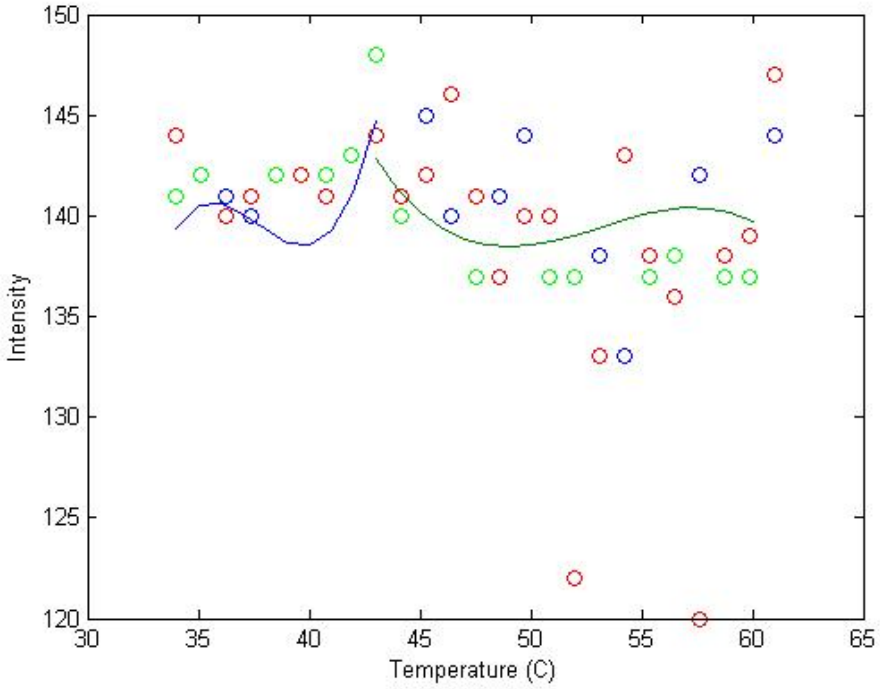

Figure 22. Polystyrene with Rhodamine 700, modeled with two third-order polynomials

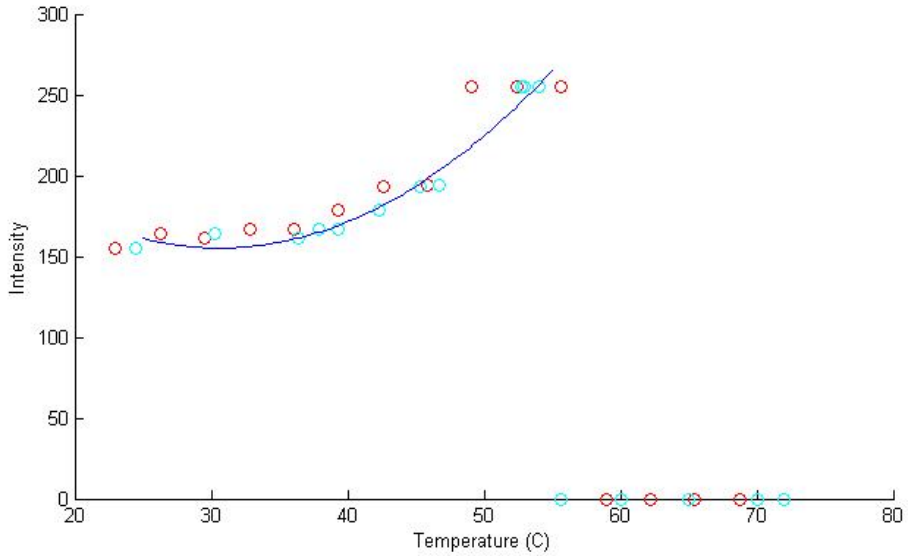

Figure 23. Polystyrene with Rhodamine 800, modeled by a parabola

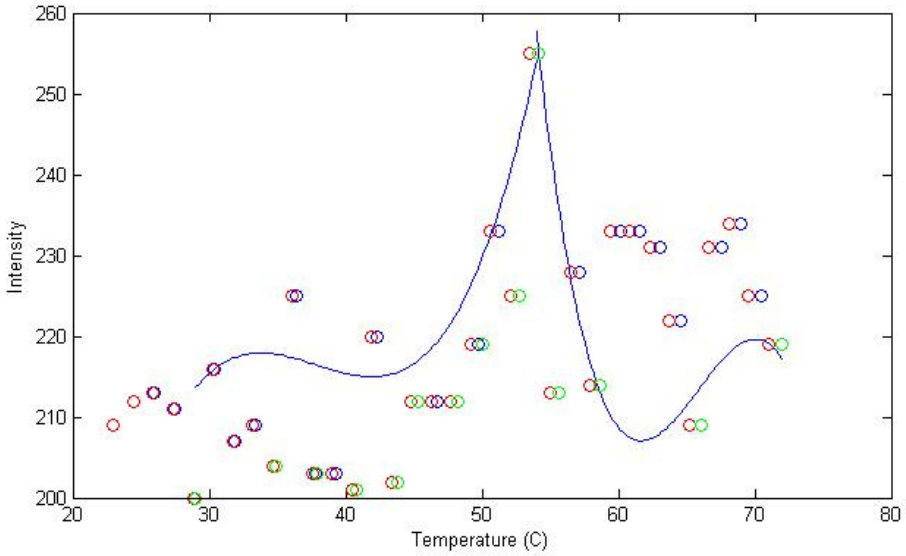

Figure 24. Polystyrene with Rhodamine 6G, modeled by two third-order polynomials

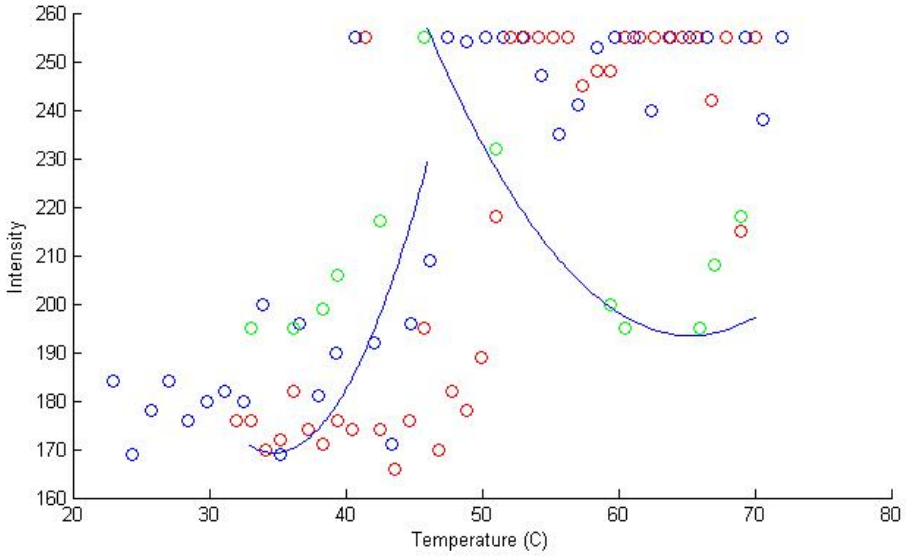

Figure 25. Polystyrene with Nile Red, modeled by two parabolas

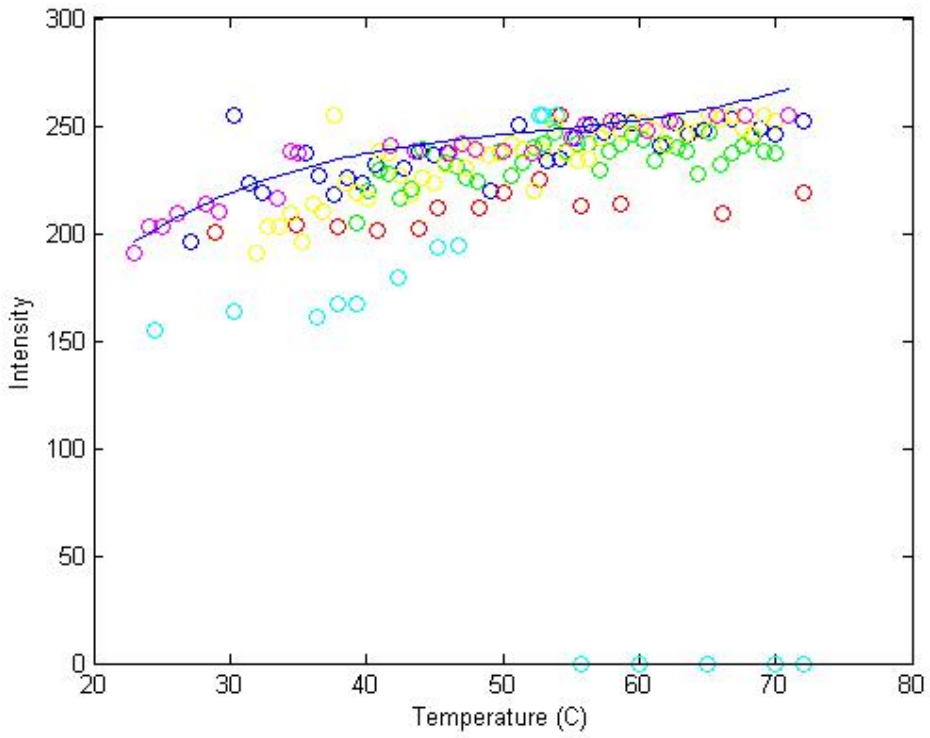

Figure 26. Polystyrene with Nile Blue, modeled by a third-order polynomial

5.2. Intensity-temperature curves for 2-(N,N-Dimethylamino) ethylmethacrylate particles

To further investigate the Nile blue intensity shape, a batch of dMMA particles with the same concentration of dye was created. This yielded a very different shape than the polystyrene particles, as seen in Figure 27. Rather than reaching a peak and decreasing, the particles experienced several peaks, which are modeled as parabolas.

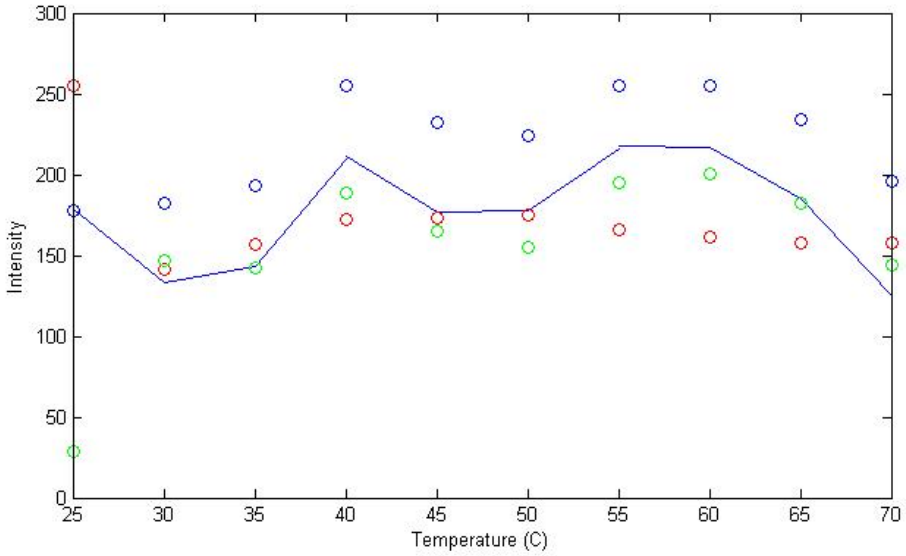

Figure 27. dMMA with Nile blue, modeled by three parabolas

5.3. Precision and uncertainty analysis

This method presents many issues. First, the limitations of the available camera make it necessary to produce polymers long enough to be seen by the camera (longer than 7.86 µm). While relationships between particle size and temperature have been established [1], the lack of fluorescence vs temperature data for many dyes does not allow for a very accurate correlation between the fluorescence intensity observed in these experiments and the expected curves for a smaller particle size. However, these results may still be useful for macroscale experiments or for later comparison between smaller molecules and those presented here.

A final shortfall to the use of these dyes involves the photobleaching effect. After exposure roughly equal to

Fluorescence intensity x emission time x number of cycles

a fluorophore will gradually be destroyed, causing the fluorescence intensity to go to zero for the remainder of the experiment [26]. Therefore, temperature determination cannot be reliable after this point in time, as the image intensity will be the same regardless of its temperature. This issue can be avoided by increasing the fluorophore concentration; namely, adding larger amounts of dye to the styrene mix prior to initiation. Here Rhodamine 800 seems to display a photo-bleaching behavior. Future work should consider the addition of more dye particles during synthesis. Nile Red also reaches a near-zero intensity after reaching its peak; however, its gradual increase after 60 C would indicate fluorophores were still present that had not been destroyed.

Phase change temperature effects are not considered here, as they complicate fluorescence plots and fluorophore concentration calculations. As the solution is 64% water, once the solvent begins to boil the remaining dyes and styrene polymers are at an increased concentration over their prior concentrations. This would artificially increase fluorescence intensity data and produce inaccurate calibration curves. Therefore, experiments are only carried out to a maximum of 80 C. This also can aid in avoiding issues with the glass-transition effects experienced by the cuvettes: as the hot plate was set at higher temperatures than the desired fluid temperatures, the cuvettes heated faster than the fluids. This caused several of the containers to warp and may have contributed to unexpected data towards the end of experiments, as seen in Figure 28. The change in intensity levels after 60 C in the Nile Red dye may be explained by this warping effect.

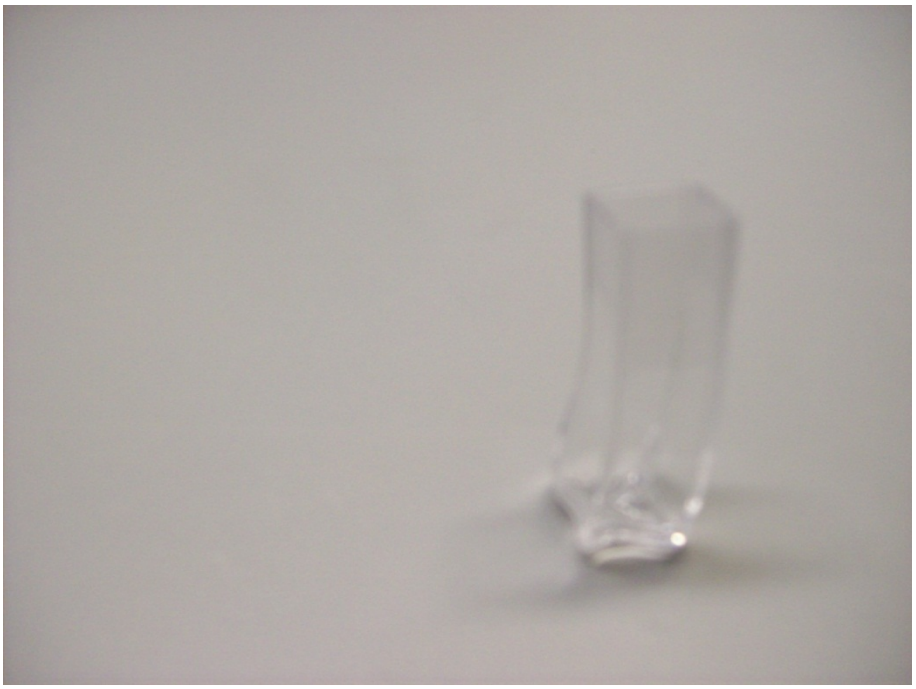

Figure 28. Warped cuvette after experiencing glass-transition temperatures

Due to the shape of the intensity plots, calibration curves are only reliable across the linear decreases observed. Temperature measurements in the domains prior to and after the discontinuity will not be reliable, as the intensity levels are roughly the same in the temperature domain above and below the temperature at which the discontinuity occurred, e.g. it would be impossible for an experimenter to establish a temperature based on the intensity observed below 50 C for rose Bengal as the intensity levels are nearly equal prior to the fluid reaching 50 C. Other elements such as camera exposure time may affect intensity readings, and should be taken into consideration prior to establishing nanoparticle temperature using this method. In addition, many of the curve fits are higher-order polynomials that would require more computationally expensive root-finding

methods to establish temperature; and in the case of higher-order polynomials would still result in multiple possible temperature values.

To establish uncertainty and error range in these measurements, MATLAB is used to determine the change in intensity values between runs for intensity values collected at the same temperature. An equation relating the uncertainty in the intensity and the uncertainty in the established temperature is derived by differentiating the applicable model for each plot and temperature range and substituting the returned values for intensity error. The inherent error in the model is considered by incorporating the R^2 metric. The values for the temperature uncertainty are presented in Table 6.

Table 6. Calculated Uncertainty Values

Dye	Uncertainty (±C)
Rose Bengal	7.579
Rhodamine 700	1.751
Rhodamine 800	3.230
Rhodamine 6G	3.227
Nile Red	5.705
Nile Blue A	12.131

Here Nile Blue A has the highest uncertainty at 12.131 C, while Rhodamine 700 holds the lowest at 1.751.

However, the plot for Nile Blue A shows some promise as it does not exhibit a parabola or concave shape similar to the other dyes. Further research should be considered to establish whether Nile Blue avoids issues with multiple temperature values experienced by the other dyes presented here. A possible explanation for its unique shape lies in the fact that it is light- and pH-sensitive

[19] and therefore could be experiencing some fluorophore deterioration and recovery as subtle changes occur over time in the sample of solution being photographed in experiments.

CHAPTER 6

CONCLUSIONS

This work describes the relationship between a variety of nanoparticle materials and laser-induced fluorescent dyes and how said relationship can be used to measure nanoparticle temperature if fluorescence intensity is known. Limitations in optical resolution capabilities can be handled by increasing nanoparticle aggregation times and therefore increasing particle diameter to visible ranges. Temperature ranges can be achieved with a hot plate, but care should be taken not to heat cuvettes or other containers beyond the glass-transition point as this can alter the optical path. These temperature models are reliable with R^2 values greater than 0.9 in most cases; however, the best curve would only apply within a specified domain of the temperature range in question and the experimenter would need to know whether the fluorophores had already reached maximum intensity to use the correct model. Thermometry measurements should not be performed outside the specified domain as this introduces inaccuracies due to the same intensity levels observed across these domains. Additionally, measurements taken beyond the fluid boiling point, or after photobleaching effects are observed, should not be considered reliable.

Although a method of establishing nanoparticle temperature through the use of the same dyes being used for intracellular tracking may be convenient, the dyes used here, with the exception of Nile Blue, are not efficient temperature sensors based on their tendency to follow parabolic or high-order models which would yield multiple temperature values in a fluorescence experiment. These results are

of particular interest in the field of fluorescence-based thermometry as they demonstrate a need for a more reliable temperature-sensitive dye that can exhibit predictable behaviors at a variety of temperatures. While the dyes used here may have relevant uses in other biological applications, they do not exhibit behaviors consistent with that of an effective temperature sensor. With the addition of further research into biological and laser dyes, a better temperature sensor may be developed that can effectively track intracellular processes as well as establishing reliable temperature values.

CHAPTER 7

FUTURE WORK

It is recommended that more particle and dye combinations be used in future work. While polystyrene is an affordable, common particle that is easy to synthesize, a broader range of carbon-based particles should be considered for biological applications. A wide variety of laser dyes exist that are temperature-sensitive and could be used for fluorescence tagging; however, there is not much literature that relates fluorescence intensity to temperature for many of these dyes. A broader knowledge of dyes and particles that can be used to produce reliable temperature calibration charts would be helpful for both medical procedures and nanoscale system monitoring.

A second element that should be introduced in future work would be a tunable excitation source such as a diode-pumped, tunable laser. This would have the added benefit of allowing the experimenter to use a broader range of dyes, as dyes requiring higher excitation energies could be considered. In addition, further inquiries into the effects of quantum efficiency could be performed, as quantum efficiency is best determined across a broad range of wavelengths for a given laser dye.

Future work could also improve in the capacity of optics technology available. Using a scanning electron microscope or other imaging technology capable of resolving images to much lower than the resolution presented here would potentially allow the experimenter to view single nanoparticles at a time, and thus determine their temperature. This could also allow the experimenter more

leverage in the synthesis of the particles, as aggregation time could be greatly reduced if smaller polymers can be viewed. This would result in a decreased turnaround time between synthesis and experimentation. Additionally, relationships between polymer length and reliability as a temperature sensor could be further investigated. Relationships between particle size and fluorescence properties could be better understood, and ideal sizes for medical procedures and other biological applications could be considered.

Finally, a greater temperature resolution could be achieved through the use of real-time video, rather than photographs, during image acquisition. This could be particularly effective with a microheater or smaller hot plate and in-situ thermocouple, as data could be collected continuously rather than discretely as presented here. A larger number of data points could reduce statistical uncertainties and meters such as standard deviation across the temperature range.

A final consideration could be the use of a different cuvette material for experimentation. During the course of the experiments presented here, hot plates regularly reached the glass transition temperature for both the polystyrene and the poly (methyl methylacrylamide) cuvettes, causing some of them to warp. This may have complicated the optical path and other properties, as the laser beam was no longer at the same angle with the camera. However, as cellular processes are not carried out at these temperatures this is irrelevant for many applications.

REFERENCES

[1] Joo, Song-Woo. Concentration-dependent fluorescence live-cell imaging and tracking of intracellular nanoparticles. Nanotechnology, 2011. Vol. 22, 235101.

[2] Kalaidzinis, Y. Multiple objects tracking in fluorescence microscopy, Journal of Mathematical Biology, 2009. Vol.1, 57.

[3] Li, D. Tracking hantavirus nucleocapsid protein using intracellular antibodies, 2010. Vol. 7, 339.

[4] Ross, D., Geitan, M., Loscasci, L. Temperature Measurement in Microfluidic Systems Using a Temperature-Dependent Fluorescent Dye. Anal. Chem. 2001, 73, 4117-4123

[5] Hanson, Willard L. Development of a Quantum Dot Mediated Thermometry for Minimally Invasive Thermal Therapy, 2009.

[6] Waters, L. C.; Jacobson, S. C.; Kroutchinina, N.; Khandurina, J.; Foote, R.S.; Ramsey, J. M. Anal. Chem. 1998, 70, 158-62.

[7] Waters, L. C.; Jacobson, S. C.; Kroutchinina, N.; Khandurina, J.; Foote, R. S.; Ramsey, J. M. Anal. Chem. 1998, 70, 5172-6.

[8] Kopp, M. U.; De Mello, A. J.; Manz, A. Science 1998, 280, 1046-8.

[9] Wilding, P.; Kricka, L. J.; Cheng, J.; Hvichia, G.; Shoffner, M. A.; Fortina, P. Anal. Biochem. 1998, 257, 95-100.

[10] Khandurina, J.; Mcknight, T. E.; Jacobson, S. C.; Waters, L. C.; Foote, R. S.; Ramsey, J. M. Anal. Chem. 2000, 72, 2995-3000.

[11] Lagally, E. T.; Medintz, I.; Mathies, R. A. Anal. Chem. 2001, 73, 565-70.

[12]Lan, Yuncheng, . Hui W, Xiaoyuan C, Dezhi W, Gang C, and Zhifeng R. Nanothermometer Using Single Crystal Silver Nanospheres, Journal of Advanced Materials, 2009. 21:1-6.

[13] Lou, J.F. Fluorescence-Based Thermometry: Principles and Applications. REVIEWS IN ANALYTICAL CHEMISTRY, 1999. Vol: 18, 4: 235 - 284

[14] Park, J.S., Choi, C.K. Temperature measurement for a nanoparticle suspension by detecting the Brownian motion using optical serial sectioning microscopy (OSSM), 2005. Meas. Sci. Technol. 16 1418–1429

[15]Omega Optical, Curve-O-Matic. Omega Optics. <omegafilters.com> Accessed 4-10-11.

[16] Invitrogen, Life Technologies. <http://www.invitrogen.com/site/us/en/home.html> Accessed 5-15-11.

[17] Chan, Y-T. and Chan, G. Multiexciton fluorescence from semiconductor nanocrystals CHEMICAL PHYSICS, 2009. 318, 15:71 - 81

[18] Jose, Jiney; Burgess, Kevin (2006). "Benzophenoxazine-based fluorescent dyes for labeling biomolecules". Tetrahedron 62: 11021.

[19] F. J. Duarte and L. W. Hillman (Eds.), Dye Laser Principles (Academic, New York, 1990).

[20] Schellenberg, J. Effects of styrene oligomers and polymers on the suspension polymerization behavior and properties of expandable polystyrene , Journal of Applied Polymer Science, 2008. Vol: 110 Issue: 1: 453 – 458.

[21] J. Maul, B. G. Frushour, J. R. Kontoff, H. Eichenauer, K.-H. Ott, C. Schade Polystyrene and Styrene Copolymers" in Ullmann's Encyclopedia of Industrial Chemistry 2007 Wiley-VCH, Weinheim.doi:10.1002/14356007.a21_615.pub2).

[22] Wako-Chem. Initiator VA-086. <http://www.wako-chem.co.jp/specialty/waterazo/image/va_086_img_big.gif> Accessed 6-8-11.

[23] Denis H. James William M. Castor, “Styrene” in Ullmann’s Encyclopedia of Industrial Chemistry, Wiley-VCH, Weinheim, 2005.

[24] J. Maul, B. G. Frushour, J. R. Kontoff, H. Eichenauer, K.-H. Ott, C. Schade Polystyrene and Styrene Copolymers" in Ullmann's Encyclopedia of Industrial Chemistry 2007 Wiley-VCH, Weinheim.

[25] Madhu, M. Comparison of an in-house PCR assay, direct fluorescence assay and the Roche AMPLICOR Chlamydia trachomatis kit for detection of C. trachomatis. Journal of Medical Microbiology, 2009. Vol. 58:7, 867-873.

[26] Micro.Magnet. Photobleaching, 2011. <http://micro.magnet.fsu.edu/primer/java/fluorescence/photobleaching> Accessed 6-16-11.

APPENDIX A

SAMPLE IMAGES

A. A sample comparison between pictures for BODIPY dye is given.

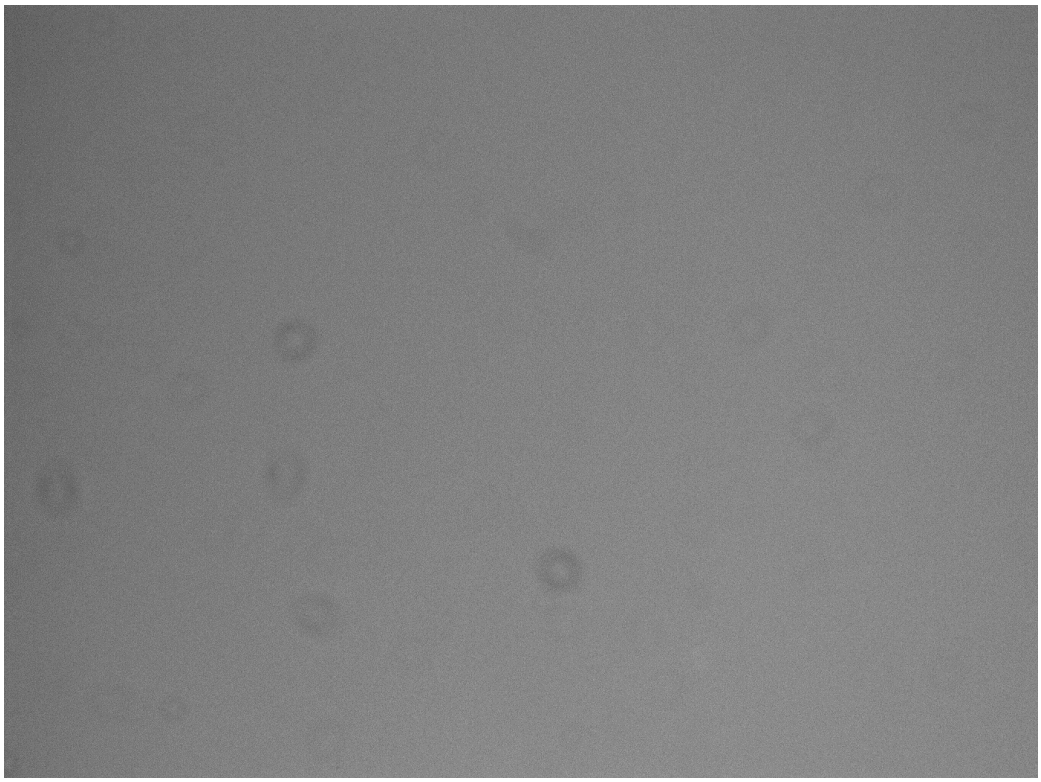

Figure A1. BODIPY prior to laser.

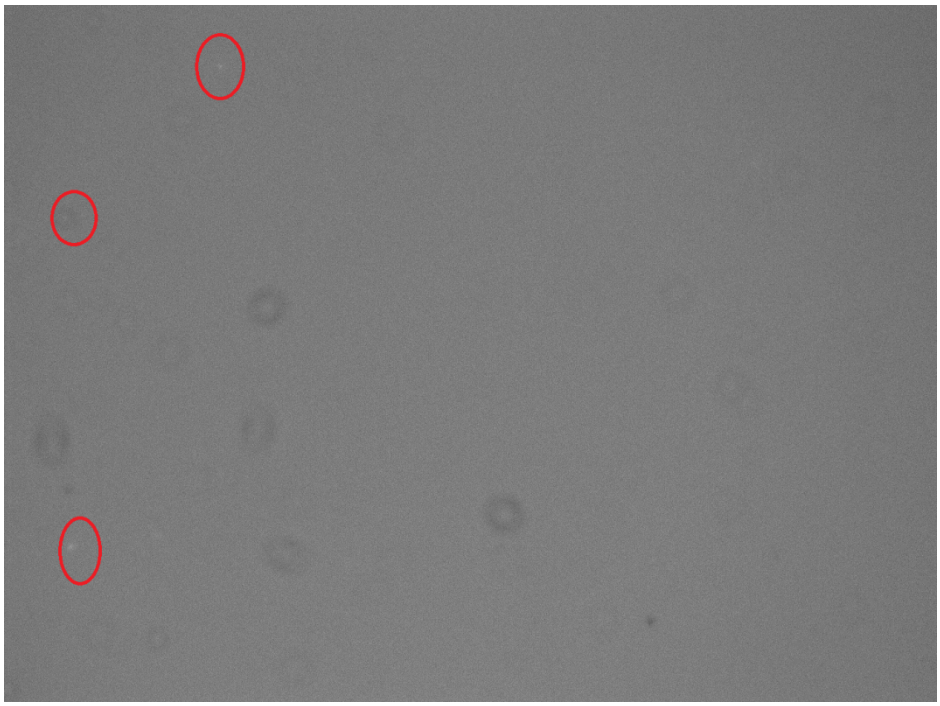

Figure A2. BODIPY dye after laser. Fluorophores circled.